Internet of Things 14 (2021) 100366

Contents lists available at ScienceDirect

Internet of Things

journal homepage: www.elsevier.com/locate/iot

UAV-Assisted Multi-path Parallel Routing for mmWave-Based Wireless Networks

Mai A. Abdel-Malek[a,1,*], Nico Saputro[b,1], Ahmed S. Ibrahim[a,1], Kemal Akkaya[a]

[a] Department of Electrical and Computer Engineering, Florida International University, Miami 33174, USA
[b] Department of Electrical Engineering, Mechatronics Program, Parahyangan Catholic University, Bandung, Indonesia

ARTICLE INFO

Article history:
Received 4 August 2020
Revised 4 January 2021
Accepted 27 January 2021
Available online 29 January 2021

Keywords:
Connectivity
End-to-end delay
mmWave
Multi-path routing
Throughput
Queuing analysis
UAV

ABSTRACT

The Millimeter Wave (mmWave) spectrum band, with its high bandwidth, will significantly satisfy the need for high data-demand of the next-generation communication networks. However, transmission over the mmWave band suffers from a short communication range due to its high frequency. Such short-range communication can dramatically affect the network connectivity in mesh-based networks, leading to excessive packet loss. To improve the network connectivity and thus the throughput, Unmanned Aerial Vehicles (UAVs)/drones can be utilized as relays. Along with UAVs, multi-path routing is needed to ensure better network reliability through different routes. In this paper, we propose maximizing mmWave-based mesh network connectivity via optimally deploying a number of UAVs/drones and enabling multiple parallel paths at the upper network layers. We model the optimization problem for minimizing end-to-end delay with a minimum number of drones, we further perform a delay analysis for the received queues and obtain the link layer end-to-end delay. The evaluation is first performed through MATLAB and then verified using a realistic scenario in the NS-3 simulator by assuming an IEEE 802.11ad-based wireless mesh network. The results show that the proposed UAV-assisted schemes achieve higher throughput and shorter delay compared to baselines scenario with no deployment of UAVs or single transmissions.

1. Introduction

The next generation of mobile networks needs to satisfy the demand for high traffic data that may emanate from the various Internet of Things (IoT) devices as well as mobile users that are increasingly demanding streaming applications [1]. Given the current wireless bandwidth crunch, [2,3], this is becoming a pressing issue that needs to be addressed for the sustainability of the current services. One of the promising solutions is to tap into higher bands, such as millimeter-wave (mmWave). Communication over the mmWave spectrum band can support such high data rates due to its abundant bandwidth [4,5].

* Corresponding author.
E-mail addresses: mabde030@fiu.edu (M.A. Abdel-Malek), nico@unpar.ac.id (N. Saputro), aibrahim@fiu.edu (A.S. Ibrahim), kakkaya@fiu.edu (K. Akkaya).

[1] The work of M. A. Abdel-Malek and A. S. Ibrahim is supported in part by the National Science Foundation under Award No. CNS-1816112 and CNS-1618692, respectively. The work of N. Sapurto is supported in Ministry of Research and Technology/National Research and Innovation Agency (Kemenristek/BRIN) of the Republic of Indonesia under the World Class Research Scheme 2020.

https://doi.org/10.1016/j.iot.2021.100366
2542-6605/

However, mmWave propagation suffers from a short communication range and can be easily blocked [6–9]. If to be used in a multi-hop wireless ad hoc network (i.e., IEEE 802.11ad/ay-based mesh network), such short-range communication may result in weak connectivity. It could even lead to a disconnected wireless network defeating the purpose of supporting high data rates [10]. Therefore, if the mmWave band is to be utilized effectively for increasing the data rate in such environments, the first challenge to be addressed is to improve the connectivity of the underlying wireless network. Once connectivity is improved, mmWave can now become a more effective means to seek throughput maximization at the upper layer of the protocol stack by potentially utilizing multiple and/or parallel transmissions through the available alternative paths.

Therefore, in this paper, we investigate how the protocol stack's upper layers can improve the mmWave network throughput, particularly in an ad hoc network where streaming might be needed in cases of emergencies or post-disaster scenarios. That not only implies enhancing the reliability of mmWave communications (i.e., reduce packet losses due to mmWave short range) but also modeling the data traffic to support more traffic within a given period. Both purposes can be achieved by relying on the deployment of additional relays in the network. The most suitable relays for wireless ad hoc networks would be Unmanned Aerial Vehicles (UAVs), as they can be used on-demand for temporary purposes. That is particularly relevant for emergency applications, military setups, or Intelligent Transportation Systems (ITS) where additional connectivity is required [11,12]. Therefore, we study the optimization problem for the deployment of UAVs to improve network connectivity. Then, we find the most appropriate routes for data transmissions that can also exploit parallel routing to boost throughput.

We consider a UAV-assisted ad hoc network with mmWave links, where we aim to enhance the network connectivity by maximizing the algebraic connectivity of the UAV-based network graph. Second, a constraint is added to limit the acceptable End-to-End (E2E) delay, and hence increase the network throughput. Jointly with choosing the minimum number of UAVs and their optimal positions, we also aim to optimally define the UAVs *transmission powers*. The problem of finding the design aspects of the UAV-based topology, as explained above, can be formulated as a complex constrained optimization problem. However, it can be relaxed to a *Semi-Definite Programming* (SDP) optimization problem, which can be solved efficiently using one of the available numerical SDP solvers.

Moreover, once the UAVs are optimally deployed, we propose forming multiple paths among each source-destination pair to provide alternative data paths in case of link failures. To this end, we propose a modified node-disjoint routing approach to minimize potential interference among inter-routes, which will enable *parallel* transmissions from the same source. In other words, we send the same packets through multiple paths simultaneously to increase the likelihood of successful reception at the receiver. To the best of our knowledge, the parallel transmission idea has not been exploited before for mmWave communications.

For the performance evaluation of the proposed approach, we used two simulation platforms. The first platform is MATLAB, which is utilized to solve the SDP optimization problem and find the deployed UAVs design parameters (3D positions and transmission powers). The second platform is the NS-3 network simulator, where we implement the IEEE 802.11*ay* mmWave communication protocol at 60 GHz, assuming an ad hoc network. Through the NS-3 simulations, we were able to show a significant increase in the network throughput while reducing the E2E delay when alternative or parallel paths are used for data transmission.

Based on the discussion aforementioned, the contributions of this paper can be summarized as follows

- We propose an analytical solution for the UAV-based *network topology formation* constrained optimization problem, where the minimum number of UAVs, along with their locations and transmission powers are identified; For this goal, we model the expected delay between a source and destination using a queuing analysis;
- We propose a multi-hop multi-path source routing scheme involving UAVs, that will also allow parallel transmissions at the network layer for increased reliability, and hence, throughput;
- We incorporate the PHY/MAC layers implementation of the IEEE 802.11ay protocol into the NS-3 simulator for developing a routing protocol with mmWave communication links and show that the developed analytical model closely matches the implementation results under NS-3.

To the best of our knowledge, we are the first work that utilizes parallel routing for mmWave communications and incorporates this idea within the IEEE 802.11ad/ay standard. The limitations on the IEEE 802.11ad are regarding the transmission range, which is within $10-20$m. However, this problem was solved in IEEE 802.11ay using MIMO technology to obtain up to 300m. Hence, since the IEEE 802.11ay implementation over NS-3 is not available to utilize yet, we utilized the IEEE 802.11ad implementation [13] and updated the physical layer to have a MIMO transmission.

The rest of the paper is organized as follows. A discussion of related works is presented in Section 2. The system model is described in Section 3. The optimization problem and the routing model are described in Section 4. Then, the proposed solution and algorithms are described in Section 5. Finally, numerical results and concluding remarks are provided in Section 6 and Section 7, respectively.

2. Related work

The research area in mmWave reliability is mostly divided into two folds. One is processing the high dropping rate for the mmWave packets through transport layer adaptation to enhance transmission reliability. The other is to tackle the mmWave short-range communication by inserting relays in the network such as reflectors or, and the most common, UAVs. Next, we

summarize current research on maintaining network connectivity through UAVs and multi-path routing efforts for improved reliability.

2.1. Network connectivity

In order to restore network functionality in mmWave communication, there is already ongoing research on utilizing UAVs as relays. That requires a rapid temporary routing algorithm toward sustainable connection to assist in retaining the communication. Many techniques have been developed to promote the selection of the UAV's position towards network supporting and enhancing the network [14,15]. Furthermore, the UAV positioning model plays a crucial role in evolving network performance [16–18]. In [19], the authors proposed an adaptive route recovery algorithm based on topology discovery and network hole replacement with UAV relays, where network hole occurs due to the terrestrial network broke links that lead to isolated sub-networks.

Optimization of 3-dimensional (3-D) positioning for UAVs has been previously considered through physical (PHY), topology, and network aspects. For instance, from the PHY perspective, maximizing the coverage radius was considered in [15]. Equivalently, enhancing the outage probability or signal-to-interference-and-noise-ratio (SINR) were discussed in [20] and [21], respectively. Achieving different data rates for different users was discussed in [22]. Finally, UAV positioning aiming to augment device-to-device (D2D) communication was considered in [23]. As opposed to these approaches, our UAV deployment is geared for maximizing reliability for mmWave communication while also minimizing the E2E delay. In this work, the optimization problem also considers the E2E delay and UAV power consumption in addition to the UAV positioning.

The second class considered UAV positioning from a topological perspective to restore network connectivity in mmWave networks. For instance, in [24], an autonomous relay scheme was proposed, and it uses mobile relays to extend the mmWave communication coverage. However, unlike this paper, where we considered the UAV placement problem, the authors only considered extending the coverage by moving a hoovering UAV around. In [25], UAVs are placed to explore ray-tracing simulations and assess Doppler effects for air to ground mmWave UAV communications. Similarly, the authors in [26] explored the blockage and Doppler effect depending on UAV positioning under mmWave spatial-division multiple access communication. As can be seen, the objective here is different from ours. In particular, we aim to optimally identify the locations for the *minimum number* of UAVs to maximize the network *connectivity*, which is needed to satisfy a particular E2E delay *constraint*. The motivation for minimizing E2E stems from the fact that increased throughput depends on the faster arrival of data; this is one of our goals.

In our previous work [27,28], we proposed optimal UAV positioning for an out-of-band cellular mmWave based 5G network. The goal in this works was to find optimal positions for UAVs to restore network connectivity for the back-haul network during break downs and at the same time act as a provider for the disconnected users in the access network. Our work here is similar in the sense that we restore connectivity. However, the application requirements and the underlying network is different (i.e., not 5G but IEEE 802.11ad/ay ad hoc network). In addition, we explore parallel multi-path routing in this work, which was not the case before.

2.2. Network routing

Furthermore, increasing network connectivity provides more routing options and enhances the communication experience with good utilization. Moreover, relying on single-path routing cannot handle the link congestion or failure, especially in ad hoc networks [29–32]. Hence, the need to have multi-path routes increases with the use of mmWave frequencies; due to its short-range and high sustainability for link failure as aforementioned.

Multi-path routing has been studied in different contexts for the traditional wireless frequencies either to enhance the link reliability or to obtain higher data rates [33,34]. More recent works are considering on-demand multi-path routing in ad hoc networks to reduce routing overheads, which have more effectiveness and efficiency [35]. With all the advantages of multi-path routing, when several paths share common resources, joint nodes, or links, performance may even degrade than single-path routing. Hence, when a link or a node is mutual among several paths, severe flow congestion occurs with high incoming traffic load. As a result, the shared node or link becomes a bottleneck [36]. Consequently, more recent research on multi-path routing proposed node-disjoint path routing protocols to avoid interference among paths [37–40]. In [41], the authors summarize the related work on multipath routing for wireless networks for both the theoretical and practical sides of multipath routing. However, our work is different in terms of the impact on the lossy mmWave network. Moreover, our optimization problem formulation for the UAV positioning considers both the E2E delay and the UAV power consumption while finding suitable multipaths for proper communication.

We propose a modified node disjoint multi-path routing algorithm, where we send the same data simultaneously to ensure a minimized packet loss and enhancement reliability.

In brief, our approach offers the following distinctions compared to the existing works: 1) While there has been some work on UAV positioning, none of the considered an optimization model that involves mmWave channels along with E2E Delay and power consumption at the same time; 2) This is the first work to offer parallel transmission to address the lossy channel issue for mmWave-based communications integrating a lower layer problem with an upper layer solution that involves transport and network layers. While multi-path routing has been used for other purposes, none of these works con-

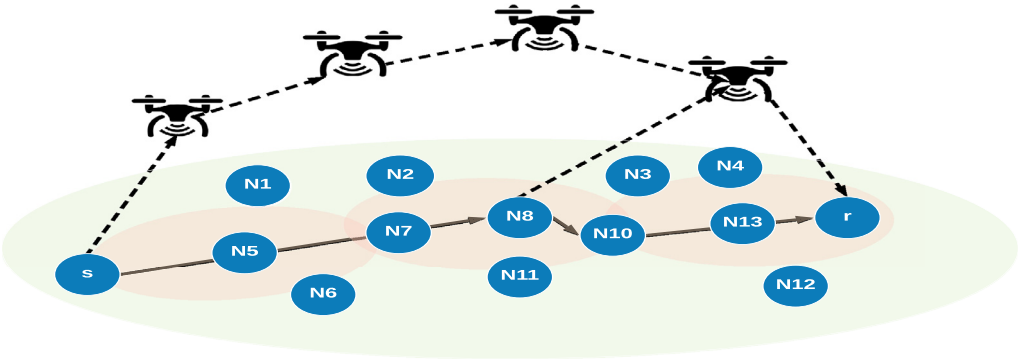

Fig. 1. System model.

Table 1
Notations.

Parameter	Definition
K_V	Number of UAVs.
N	Number of nodes in the network.
s	Transmitter node.
r	Receiver node.
n	Path loss exponent.
$SINR_r$	Signal to interference-plus-noise ratio at the receiver.
$R_{s,r}$	Maximum rate between the transmitter and receiver.
W	MmWave transmission bandwidth.
f	MmWave transmission frequency.
D_{E2E}	End-to-End delay between the transmitter and receiver nodes.
(M/G/1,....)	Markov chain standard representation for the queue type.
$\lambda_2(L)$	Algebraic connectivity (Fiedler value) of a graph that represents a network.
P_V	UAV maximum transmission power
D_{th}	E2E delay threshold.

sidered exploiting parallelism for addressing mmWave issues; and 3) We are the first to provide an actual implementation of mmWave in NS-3 to provide a realistic framework.

3. System model

Fig. 1 depicts the assumed system model of an ad hoc wireless mesh network, which consists of N nodes. A number of UAVs, K_V, are deployed to increase network connectivity. Each wireless link is assumed to utilize the mmWave frequency band at a frequency of 60 GHz. Before we detail the link model, delay model, and network model that are used later in the computation of the number and locations of the UAVs, we also briefly define the used notation as follows:

Lower- and upper-case bold letters denote vectors and matrices, respectively, while $\mathbf{I}_M$ denotes the identity matrix of size M. The operations $(\cdot)^T$, $\mathbb{E}[\cdot]$, and $|\cdot|$ denote the transpose, statistical expectation, and absolute value, respectively. The $\mathbf{A} \preceq \mathbf{B}$ denotes that $\mathbf{B} - \mathbf{A}$ is a positive semi-definite matrix. Finally, $\otimes$ denotes the Kronecker product operation. The main parameter notations used through the paper are listed in Table 1.

3.1. mmWave channel model

We consider a 60 GHz mmWave channel model for both the small scale and large scale fading [42], where the authors addressed the channel variation and beamforming tracing for both line-of-sight (LoS) and non-line-of-sight (NLoS). The fluctuation and beamforming model is then addressed in the channel coefficient representing the mmWave ray tracing. Then, the received baseband signal from a source, s, at a destination, r, within a transmission radius R is as follows:

$$y_r = \sqrt{P_{i,r}} h_{i,r} d_{i,r}^{-n/2} x_{s,r} + \sum_{j=1, j\neq i}^{N} \sqrt{P_{j,r}} h_{j,r} d_{j,r}^{-n/2} x_{j,r} + n_0, \tag{1}$$

where $p_{i,r}$ is the transmitted power from the last node in the path i to the destination node r and $p_{j,r}$ is the transmitted power from any other node j to the destination node r which is considered as interference to node r. $x_{s,r}, x_{j,r}$ are the transmitted unit-power symbols from node s and j to node r, respectively, and $d_{i,r}, d_{j,r}$ represent the distance between i and j nodes and r. Moreover, n_0 denotes zero-mean circularly-symmetric additive-white-Gaussian noise (AWGN) with variance

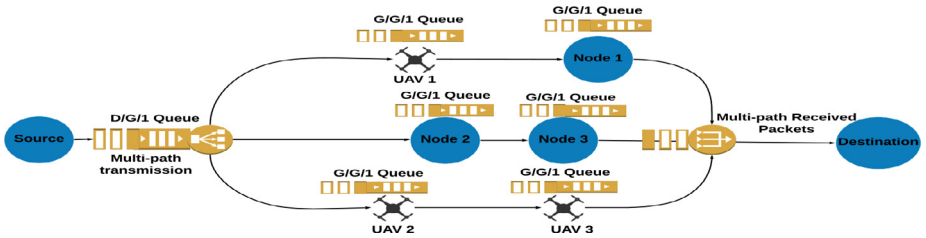

Fig. 2. Multi-path queuing model.

σ_0^2 and it is assumed to be independent across the nodes. Furthermore, $h_{i,r}$ and $h_{j,r}$ are the channel coefficient representing the small scale fading corresponding to the channel between node i and r, or node j and r, respectively. Finally, n is the path loss exponent.

The signal to interference-plus-noise ratio (SINR) at the input of the receiver is given by

$$\text{SINR}_r = \frac{P_{i,r}|h_{i,r}|^2 d_{i,r}^{-n}}{\sum_{j=1,j\neq i}^{N} P_{j,r}|h_{j,r}|^2 d_{j,r}^{-n} + \sigma_0^2}. \tag{2}$$

Following an information-theoretic model, the maximum rate for the communication between nodes r and s is computed as

$$R_{s,r} = W \log_2 \left(1 + \frac{P_{i,r}|h_{i,r}|^2 d_{i,r}^{-n}}{\sum_{j=1,j\neq i}^{N} P_{j,r}|h_{j,r}|^2 d_{j,r}^{-n} + \sigma_0^2}\right), \tag{3}$$

where W is the transmission bandwidth for the mmWave standard.

3.2. Delay link model

In this section, we model the expected delay for a packet between the source and the destination which may include multiple intermediate hops. The E2E delay can be written as [43],

$$D_{E2E} = D_t + D_p + D_q, \tag{4}$$

where D_t, D_P and D_q are the transmission delay, propagation delay and queuing delay, respectively. Moreover, the transmission delay, D_t, represents the time required to put an entire packet into the communication media and can be written as,

$$D_t = N' \frac{m}{\min_{\{i,j\}\in \mathbf{s}} R_{i,j}}, \tag{5}$$

where, N' is the number of nodes in the route between the source and the destination nodes, m is the packet size and $\mathbf{s}$ is the set of nodes in the source and destination route including the UAVs.

The propagation delay, D_p, is the time that takes a signal to propagate through the communication media from one node to the next one and can be written as,

$$D_p = \frac{\sum_{\{i,j\}\in \mathbf{s}}^{N'} \|\mathbf{u}_i - \mathbf{u}_j\|_2}{c}, \tag{6}$$

where $\mathbf{u}_i = [X_i, Y_i, Z_i]$ and $\mathbf{u}_j = [X_j, Y_j, Z_j]$ are the i^{th} and j^{th} nodes 3×1 position vector in the Cartesian coordinate system, respectively.

Furthermore, the queuing delay, D_q, is the waiting time for the packet spent in a queue to be transmitted, which is usually obtained by performing queue model analysis [44]. This type of analysis includes an investigation of the status of the arriving packet queue and the service/drain rate, as shown in Fig. 2.

After investigating the queue model at the source point, we considered a queue of $M/G/1$ model. The queue has a Poisson distribution with λ_i arrival rate at the i^{th} node represented by the symbol 'M' and a general service rate depending on the mmWave channel between the source node and the next hop represented by the symbol 'G'. Moreover, towards our aim for a reliable mmWave network, each packet from the source is to be transmitted on all the available multi-paths. In other words, in the queuing model, we copy the queue output to all the available paths instead of splitting the queue for all the multi-path connections. Hence, our model is $M/G/1$ and not $M/G/M$, where M is the number of available multi-paths. The $M/G/1$ model is a Markov chain standard representation for the queue type depending on the input and output rates, shown in Fig. 3.

Furthermore, all the nodes in the path except for the source node have a $G/G/1$ queuing model as the arrival rate depends on the arrived packets through the channel.

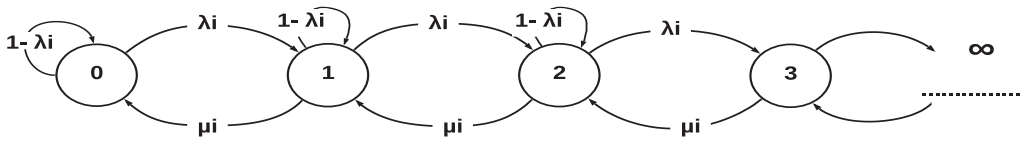

Fig. 3. Markov chain representation for M/G/1 and G/G/1.

Then, the queuing delay at the source point is given by

$$W_s = \frac{\lambda_i(\sigma_X^2 + \mathbf{E}\{X\}^2)}{2(1-\rho)} + \frac{1}{\mu_i}. \tag{7}$$

where λ_i, $\mathbf{E}\{X\}$ and σ_X^2 are the arriving rate to the source node queue, the service process expectation, and variance at node i which is the source node in this case, respectively. Moreover, $\rho = \lambda_i/\mu_i$ is the service utilization, where μ_i is the service rate of the queue and $0 \leq \rho < 1$.

The total delay at any node i (except the source node s) is as follows (see Appendix I for more detailed explanation):

$$W_i = \sigma_Y^2 \left(\frac{d_{r,i}}{d_{s,i}|d_{s,i} - d_{r,i}|} \right)^n + \mathbf{E}\{Y\} d_{s,i}^{-n}, \tag{8}$$

where $\mathbf{E}\{Y\}$ and σ_Y^2 are the expectation and the variance of the queue service process, respectively. Moreover, $d_{s,i}$ and $d_{r,i}$ are the distance between the source s or the destination r and the i^{th} node in the network, respectively. Hence, the total queue delay on any path is:

$$D_q = \min_M \left(\sum_{i=1}^{N'} W_i + W_s \right). \tag{9}$$

where M is the number of available paths.

3.3. Graph-theoretic network model

The baseline network can be modeled as an undirected finite graph $\mathcal{G}(\mathbf{V}, \mathbf{E})$, where $\mathbf{V} = \{v_1, v_2, \cdots, v_N\}$ is the set of the N nodes constructing the network and $\mathbf{E} = \{e_1, e_2, \ldots, e_Q\}$ is the set of all Q edges (links). For an edge q, $1 \leq q \leq Q$, connecting nodes $v_i, v_j \in V$, we define the corresponding edge vector $\mathbf{a}_q \in \mathbf{R}^{N\times 1}$, where the i^{th} and j^{th} elements are given by $a_{q,i} = 1$ and $a_{q,j} = -1$, respectively, and the rest is zero. The relationship between the N vertices and the corresponding Q links between those vertices in $\mathcal{G}$ is captured in a matrix named the incidence matrix $\mathbf{A} \in \mathbf{R}^{N\times Q}$, where the q^{th} column is given by $\mathbf{a}_q$. For this undirected graph, the Laplacian matrix $\mathbf{L}(\mathbf{A}) \in \mathbf{R}^{N\times N}$ is defined as:

$$\mathbf{L}(\mathbf{A}) = \mathbf{A}\mathbf{A}^T = \sum_{q=1}^{Q} \mathbf{a}_q \mathbf{a}_q^T. \tag{10}$$

The Laplacian matrix for such graph is positive semi-definite, which is expressed as $L \succcurlyeq 0$ and also the smallest eigenvalue is zero, i.e., $\lambda_1(L) = 0$. The second smallest eigenvalue of L, $\lambda_2(L)$, is the algebraic connectivity of the graph $\mathcal{G}$ also called Fiedler value [45], which will be used in the rest of this paper to represent the network connectivity.

A UAV, as a hovering relay, can relay data packets between two nodes in the network. Accordingly, deploying a UAV can create one or more links (edges) in the baseline graph $\mathcal{G}(\mathbf{V}, \mathbf{E})$, which results in a new graph $\mathcal{G}'(\mathbf{V}, \mathbf{E}')$. The new graph $\mathcal{G}'$ has the same number of N nodes, but with a larger set of edges denoted by $\mathbf{E}'$ with Q' edges where $Q' \geq Q$, i.e., $\mathbf{E} \subseteq \mathbf{E}'$. The potential increase in the network connectivity, due to deploying UAVs, can be computed as $\lambda_2(\mathbf{L}') - \lambda_2(\mathbf{L})$.

4. Problem motivation and formulation

4.1. Motivation

The motivation behind combining the UAVs' deployment and multiple paths is based on the potential impact of the upper layers for routing on enhancing the mmWave channel behavior. To demonstrate this, we conducted a simple experiment where IEEE 802.11g and IEEE 802.11ay MAC layer are used for routing in an ad hoc network. We created a 10-node ad hoc network topology in the NS-3 simulator and established 3 different routes from a source to its destination. We transmitted data from the source to the destination under different path loss exponents using Transmission Control Protocol (TCP) as the transport layer protocol. The results for packet delay are shown in Table 2. From these results, we can see that the E2E delay when IEEE 802.11g is used is higher, but there is always a successful packet routing. On the other hand, when IEEE 802.11ay

Table 2
Comparison of 802.11 g at 2.4 Ghz and mmWave at 60 Ghz.

Path Loss	E2E Delay (ms)					
Exponent	IEEE 802.11 g			IEEE 802.11 ay		
(n)	Path 1	Path 2	Path 3	Path 1	Path 2	Path 3
2	1.65	1.12	1.67	0.34	0.234	0.348
3	1.65	1.12	1.67	0.34	N/A	0.4122
4	1.65	1.12	1.67	N/A	N/A	N/A

is used, we observe reduced E2E delay due to the higher transmission rate. However, the packet receiving is not always guaranteed, even though TCP is used to ensure re-transmissions in case of failures. For instance, under $n = 4$, no routes were successful in transporting the packets. These results suggest that under mmWave channels, the three routes need to be available for backup, and even this may not be enough (i.e., see the case when $n = 4$), and thus additional relays might be needed. Connectivity becomes a crucial concern to be able to benefit from high-bandwidth mmWave communications. Next, we formulate our problem to address the aforementioned concerns.

4.2. Problem formulation

First, we introduce the optimization problem to enhance the network connectivity with a maximum allowed constraint on the E2E delay between the desired source and destination. We also consider finding the minimum number of K_V UAVs, the UAVs' optimal locations, and transmission power.

Mathematically, this optimization problem can be formulated as follows:

$$\begin{aligned} \max_{\mathbf{U}, P_q, K_V} \quad & \lambda_2(\mathbf{L}'(\mathbf{U})) \\ \text{s. t.} \quad & D_{E2E} \leq D_{\text{th}}, \\ & d_{i,j} \leq R, \\ & \textstyle\sum_{q=1}^{Q_V} P_q \leq P_V, \end{aligned} \tag{11}$$

where $\mathbf{U}$ is the $3 \times K_V$ UAVs position matrix in the Cartesian coordinate system and D_{th} is the E2E delay threshold. In this work, we consider the Cartesian coordinates to specify the UAV position and transmission direction, hence, we assume a fixed UAV antenna angle. Moreover, $d_{i,j}$ where $i, j \in 1, 2, \ldots, K_V$ denotes the distance between any 2 UAVs i and j. The maximum UAV transmission power is P_V, and P_q is the UAV transmission power over each link q of Q_V, which represents the total number of links provided by the UAV.

Once the UAVs are deployed through the optimization problem, we tackle the improving reliability at the network layer problem. In order to increase the network reliability for mmWave communication, a modified node-disjoint routing multi-path protocol is proposed. Note that the same data will be sent through all these node-disjoint paths simultaneously to increase the success rate. In this way, the receiver can also select the minimum E2E delay path for multiple packets that arrive for the same data. This approach also minimizes the potential interference among inter-routes since the same nodes and links are not shared by different routes.

5. Proposed solution

In this section, we describe, in detail, the proposed solutions and algorithms to find the optimal UAVs' positions and the multi-path/parallel routing between a particular source and a destination. The optimization problem solution is detailed in Algorithm 1 in Section 5.1 while the routing technique is detailed in Algorithm 2 in Section 5.2.

5.1. Connectivity optimization relaxation and solution

To address the indirect relation between the graph Laplacian matrix and the UAVs position, we use a quantized grid such that the nodes are distributed over $h \times h \times h$ volume. Moreover, the search space over the x, y, and z axes is uniformly quantized with a step size δ to get a search grid consisting of β candidate positions for the UAV. This simplifies the Laplacian matrix to be represented by the following formula:

$$\mathbf{L}' = \mathbf{L} + \sum_{j=1}^{\beta} x_j \mathbf{A}'_j \mathbf{A}'^T_j, \tag{12}$$

where $\mathbf{L}$ is the original graph before UAV deployment, and x_j is equal to one if a UAV is positioned in the j^{th} grid point, otherwise $x_j = 0$. Moreover, $\mathbf{A}'_j$ is the incidence matrix when the UAV is deployed in this grid point.

Collecting x_j, $j \in \{1, \ldots, \beta\}$, in the $\beta \times 1$ vector $\mathbf{x}$, Eq. (12) can be written as follows:

$$\mathbf{L}' = \mathbf{L} + (\mathbf{x} \otimes \mathbf{I}_M)\mathbf{\Gamma}, \tag{13}$$

Algorithm 1 UAVs Positioning.

Input: $(\mathbf{X}, \mathbf{Y}, \mathbf{Z})$ and $K_V = 1$
$\mathbf{A} \leftarrow$ the graph incidence Matrix
$\lambda_2(\mathbf{L}(\mathbf{A})) \leftarrow$ Network connectivity of $\mathcal{G}$
$K \leftarrow$ The maximum available UAVs
Quantize:
$\beta \leftarrow$ Grid positions; $\mathbf{x} \leftarrow \beta \times 1$ vector
$Perm(\beta) \leftarrow$ permutation of all grid positions
for $\forall K_V \leq K$ & $\forall P(\beta)$ **do**
    Link Matrix:
    $A'(\mathbf{x}) \leftarrow$ Link matrix after adding *UAVs*
    $\mathbf{L}'(\mathbf{x}) \leftarrow$ Laplacian matrix after adding*UAVs*
    $E2E \leftarrow$ The E2E delay
end for
Optimization:
$\max_{\mathbf{x}} \quad \lambda_2(\mathbf{L}'(\mathbf{A}'(\mathbf{x})))$
if $\mathbf{x}^T\mathbf{b} \leq D_{th}$ & UAV total power $\leq P_V$ **then**
    Break
else
    goto *Optimization*.
    $(X_V, Y_V, Z_V) \leftarrow \max_{\mathbf{x}}$.
end if
Loop:
if $d_{i,j} > R$ **then**
    $K_V \leftarrow K_V + 1$
    $(X_V, Y_V, Z_V) \leftarrow \max_{\mathbf{x}}$.
    goto *Loop*.
end if
Output: $(\mathbf{X_V}, \mathbf{Y_V}, \mathbf{Z_V})$, P_q and K_V

Algorithm 2 Multi-path Routes.

Input: $(\mathbf{X}, \mathbf{Y}, \mathbf{Z})$, $(\mathbf{X_V}, \mathbf{Y_V}, \mathbf{Z_V})$, D_{th} and K_V
$Q'' \leftarrow$ The total number of links after adding the UAVs
$\mathcal{G}'' \leftarrow (\mathbf{V}'', \mathbf{E}'')$ The network graph including the UAVs
root $\leftarrow$ The source node s
$\mathbf{t} \leftarrow []$ initial empty spanning tree
$\mathbf{c} \leftarrow$ Initial cost $= 0$
for $i \leq N + K_V$ **do**
    if *root* $\notin \mathbf{t}$ **then**
        $\mathbf{t} \leftarrow$ *root*
        $\mathbf{c} \leftarrow \mathbf{c} + D_{E2E}$
    end if
end for
TC $\leftarrow$ Total Cost vector on all the paths
ST $\leftarrow$ Spanning Tree
for $\forall \mathbf{t} \in \mathbf{ST}$ **do**
    if $\mathbf{ST} \cap \mathbf{t} \neq \Phi || \mathbf{c} > D_{th}$ **then**
        $\mathbf{ST} \leftarrow \mathbf{ST} - \mathbf{t}$
        $\mathbf{TC} \leftarrow \mathbf{TC} - \mathbf{c}$
        $H \leftarrow$ The number of hops $\forall \mathbf{ST}$
    end if
end for
$\mathbf{path}_i \leftarrow \mathbf{ST}|_{\min(H,c)}$
for $\forall$ **ST do**
    if $[N+1 : N+K_V] \in \mathbf{ST}$ & $\mathbf{ST} \cap [1 : N] - [s, r] = \Phi$ **then**
        $\mathbf{path}_{i+1} \leftarrow \mathbf{ST}|_{\min(H,c)}$
    end if
end for
Output: $\mathbf{path}_1, \mathbf{path}_2, \ldots, \mathbf{path}_i$.

where $\mathbf{\Gamma} \triangleq \left[\left(\mathbf{A}'_1\mathbf{A}'^T_1\right)^T, \ \ldots, \ \left(\mathbf{A}'_\beta\mathbf{A}'^T_\beta\right)\right]^T$

Furthermore, we apply the quantized grid model over the E2E delay in a $\mathbf{b} \in \mathbf{R}^{\beta\times 1} = [b_1, b_2, \ldots, b_\beta]^T$ such as

$$b_i = D_{E2E}|_{\beta=i}. \tag{14}$$

where $\mathbf{b}$ is the vector of the minimum E2E delay over all the available paths through the destination for all the β possible UAVs positions.

Hence, the optimization problem can be written in terms of the UAVs position index vector $\mathbf{x}$ rather than its actual 3-D physical locations as follows:

$$\begin{aligned} \max_{\mathbf{x},P_q,K_V} \quad & \lambda_2(\mathbf{L}'(\mathbf{x})) \\ \text{s. t.} \quad & \mathbf{x}^T\mathbf{b} \le D_{\text{th}}, \\ & \mathbf{x}^T\mathbf{d}_{i,j} \le R, \\ & \textstyle\sum_{q=1}^{Q_V} P_q \le P_V, \\ & \mathbf{x} \in \{0,1\}, \end{aligned} \tag{15}$$

where, $\mathbf{d}_{i,j}$ is $\beta \times K_V$ matrix representing the distance between any 2 UAVs. Furthermore, the first constraint $\mathbf{x}^T\mathbf{b} \le D_{\text{th}}$ represents the E2E delay constraint, where $\mathbf{b}$ is the vector of the E2E delay over all the available paths through the destination.

Moreover, $\lambda_2(\mathbf{L}'(\mathbf{A}'(\mathbf{x})))$ can be written as the point-wise infimum of a family of linear functions of $\mathbf{x}$ as:

$$\lambda_2(\mathbf{L}'(\mathbf{A}'(\mathbf{x}))) = \inf_y [y^T\mathbf{L}'(\mathbf{A}'(\mathbf{x}))y, \parallel y \parallel_2 = 1, \mathbf{1}^T y = 0]. \tag{16}$$

Hence, it is a concave function in $\mathbf{x}$. The optimization problem can be written as follows:

$$\begin{aligned} \max_{\mathbf{x},\log(P_q),K_V,\gamma} \quad & \gamma \\ \text{s. t.} \quad & \gamma(\mathbf{I} - \tfrac{1}{\beta}\mathbf{1}\mathbf{1}^T) \preceq \mathbf{L}'(\mathbf{x}, P_q, K_V) \\ & \mathbf{x}^T\mathbf{b} \le D_{\text{th}}, \\ & \mathbf{x}^T\mathbf{d}_{i,j} \le R, \\ & \textstyle\sum_{q=1}^{Q_V} P_q \le P_V, \\ & \mathbf{1}^T\mathbf{x} <= K_V, \ \ \mathbf{x} \in [0,1]. \end{aligned} \tag{17}$$

Investigating the problem convexity, the objective function, γ, is linear in the optimization variables. Moreover, the first constraint is a semi-definite constraint. The second constraint, $\mathbf{x}^T\mathbf{b} \le D_{\text{th}}$ is also a linear constraint in its general form as proven in details in Appendix II.

In addition, the rest of the constraints are linear in $\mathbf{x}$. Therefore, the optimization problem is a convex optimization problem with linear constraints. The optimization problem in Eq. (17) can be written as a Semi-definite Programming (SDP), a sub category of the convex optimization, after relaxing the binary constraint in $\mathbf{x}$ to be real value between 0 and 1, as follows:

$$\begin{aligned} \max_{\mathbf{x},\log(P_q),K_V,\gamma} \quad & \gamma \\ \text{s. t.} \quad & \gamma(\mathbf{I} - \tfrac{1}{\beta}\mathbf{1}\mathbf{1}^T) \preceq \mathbf{L}'(\mathbf{x}, P_q, K_V) \\ & \mathbf{x}^T\mathbf{b} \le D_{\text{th}}, \\ & \mathbf{x}^T\mathbf{d}_{i,j} \le R, \\ & \textstyle\sum_{q=1}^{Q_V} P_q \le P_V, \\ & \mathbf{1}^T\mathbf{x} <= K_V, \ \ 0 \le \mathbf{x} \le 1. \end{aligned} \tag{18}$$

The relaxed SDP problem in Eq. (18) can be solved using an *SDP* solver such as CVX SDPT3 solver [46].

Algorithm 1 summarizes the solution presented above as follows: The first step is to quantize the 3-D grid to the $h \times h \times h$ cubs. In the next step, every time a UAV is added to the grid, a new graph incidence matrix $A'(x)$ is reconstructed for all the permutations $Perm(\beta)$ of all possible UAV positions on the grid. Additionally, the distance matrix $\mathbf{D}$ of the network is established for all $Perm(\beta)$. The algorithm, then, strives to optimize the maximum network connectivity that satisfies the requirement of the network E2E delay to be less than D_{th} by adding more UAVs. After the optimization is done and all the UAVs' positions are found in the grid, a post-processing algorithm is performed to obtain the UAVs' Cartesian coordinates by choosing the maximum K_V elements in $\mathbf{x}$.

5.2. Parallel multi-path routing

After the UAVs' positions have been determined, the next step is to find the multi-path routing to increase the reliability of the mmWave links. The aim is to increase the network reliability for the mmWave communication by sending the same data packets in parallel over multiple alternative paths.

Sending packets through multiple paths will be challenging at the upper layers in terms of implementation. For instance, if TCP is to be used, some changes will be needed since TCP establishes a connection that is maintained during data transmission at all times. If a node has multiple IP interfaces, the current multi-path TCP (MPTCP) standard [47] can be utilized

for parallel transmission. However, in our case, drones and other mobile nodes may not have such resources, and thus, new approaches are needed.

To this end, we assume that a node will use source routing (such as dynamic source routing (DSR) [48,49]) to pick among multiple available paths, labeling them separately just like multi-protocol layer switching (MPLS)-based routing [50,51]. Those labels can be incorporated in the TCP header's unused bits so that the receiving party can differentiate between different route packets. In the case of User Datagram Protocol (UDP), there is still a need for MPLS with fewer bits needed to be added to the UDP header.

We propose a multi-path protocol that is a modified node-disjoint routing approach to minimize potential interference among inter-routes; to enable parallel transmissions from the same source. In this setting, original network nodes are allowed to be used only once, while UAVs are considered to be reusable on several paths. The justification of such a model is that the UAVs are movable and adjustable to avoid link failure, whereas the nodes in the network can not be easily adjusted. Here, we propose an algorithm to determine the available paths that are independent of each other (i.e., they do not share any links or intermediate nodes) so that there will be very diverse options to send the packets, increasing the chances to make it to the receiver. Note that, given that all the nodes and their locations are known in advance; then, this will be a centralized algorithm running at the source node, which is in line with the source routing concept we offer. Basically, the source will determine the routes, label each route, and maintain them locally. Whenever a packet is to be sent, the route will be included in the packet header.

The proposed algorithm to find the multiple paths is shown in Algorithm 2. In this algorithm, an undirected finite graph $\mathcal{G}''(\mathbf{V}'', \mathbf{E}'')$ is created to represent this new network topology that consists of the original network and the deployed UAVs. $\mathbf{V}'' = \{v_1, v_2, \ldots, v_{N+K_V}\}$ is the set of the N nodes constructing the original network and $\mathbf{E}'' = \{e_1, e_2, \ldots, e_{Q''}\}$ is the set of all Q'' edges (links). The new graph $\mathcal{G}''$ is different from $\mathcal{G}'$ in the connectivity calculations as it has $N + K_V$ nodes.

Moreover, the weights of each link represent the E2E delay of the data transmission over this link. Our algorithm will find all the spanning trees, **ST**, and the corresponding cost (E2E delay) for each tree, **TC**, between the source s and destination r. Next, we only choose the spanning trees with disjoint vertices (except for the UAVs) and have a total cost less than the E2E delay threshold, D_{th}. Finally, we select the i routes with the lowest number of hops to be our paths of transmission, $\mathbf{path}_1, \mathbf{path}_2, \ldots, \mathbf{path}_i$.

By using the constraint in Eq. (18):

$$\mathbf{x}^T \mathbf{d}_{i,j} \leq R \tag{19}$$

a direct path over the UAVs can be formed as a backup route that guarantees the independence of this route from any other routes uses existing nodes. Thus, potential link failures that may happen within the existing network among the nodes will not impact this route. Finally, while power consumption is vital in the UAV deployment optimization, once they are on-site, they can be replaced when their batteries approach critical levels.

6. Performance evaluation

6.1. Simulation setup

In this section, we present the simulation results to demonstrate the effectiveness of the proposed scheme. The two algorithms presented in Section 5 are first implemented in MATLAB to obtain the UAVs' positions and the multi-path routes. Then, for testing our model in a realistic scenario, the obtained data from MATLAB is fed into a widely used NS-3 simulator to calculate the actual throughput and E2E delay. The optimization approaches are implemented in MATLAB R2016a using the CVX solver.

For NS-3, we used version 3.26 and have adopted the IEEE 802.11ad implementation described in [13] and updated the physical layer to match the IEEE 802.11ay MIMO transmission. To the best of our knowledge, this is the first multi-hop implementation of IEEE 802.11ad/ay in NS-3.

The system parameters used throughout the experiments for MATLAB and NS-3 are listed in Table 3. N nodes are deployed with a uniform random distribution within an area of 100×100 m. For the evaluation on NS-3, we created a scenario to send data between a source and destination over multi hops using the same setting as in the MATLAB evaluation. As mmWave is a better match for high-bandwidth traffics, we investigated the proposed approaches under the high-rate multimedia transmission. We utilized the *Evalvid* tool-set [52] that is designed for video management. In this scenario, the **highway** reference video from Evalvid which is around 290 MB and consists of 2000 frames, is used as the multimedia traffic.

The following metrics are used to evaluate our approach:

- *Connectivity*: The connectivity, $\lambda_2(\mathbf{L}(\mathbf{x}))$, refers to Eq. (10) used in Section 3.3. That parameter not only shows whether the nodes are highly connected or not but also indicates the level of connectedness. This parameter demonstrates the effectiveness of the optimal positioning optimization problem in Eq. (11). The increase of this parameter indicates better coverage between nodes in the network, and hence, a better communication performance.
- *E2E Delay*: This is the total delay between the source and the destination nodes. In MATLAB, we calculate the E2E delay as in Eq. (4) in Section 4. In NS-3, it is calculated from the receiver's perspective after receiving the real packet from the sender. The effectiveness of our proposed routing solution along with the optimal position reflects in a better E2E delay.

Table 3
Simulation parameters.

Parameter	Value
MATLAB Parameters	
W	2.16 GHz
f	56.16 GHz
P_V	30 dBm
σ_0^2	-130 dBm
n	4 (suburban environment)
D_{th}	3 ms
NS-3 Parameters	
Simulation time	10 sec
Video size	290 MB
Number of frames	2000
Image resolution	352×288
Frame size	30 fps
Modulation and Coding Scheme (MCS)	$18 - 25$
PHY Type	"DMG-MCS"
Antennas	1
Antenna Sectors	3
Transmission (Tx) Power	10 dBm
Tx Gain	23
Rx Gain	23

- *Throughput*: The throughput is used within NS-3 to represent the number of bits successfully received at the receiver side in a second.

6.2. Baselines for comparison

We consider two types of network topologies. The first type is the original network before the UAV deployment, while the second type is the network with UAVs after the optimization. In these networks, the following paths are compared:

- *Baseline path*: refers to the shortest path in the original network to reach the destination;
- *Hybrid path*: refers to the optimized path with the minimum number of hops that includes the node(s) in the original network and UAV(s) to reach the destination.
- *UAV-only path*: refers to the path that uses only UAV(s) to reach the destination. This path type is critical when there are not enough number of nodes to form an adequate route.
- *Parallel Multi-path*: This path represents the multi-path communication where the data is sent over both the Hybrid and UAV-only paths in parallel to ensure reliability.

6.3. Performance results

6.3.1. UAVs Placement evaluation

We considered several network topologies with a different number of nodes, and we computed the optimal number and the UAVs' location.

To initially investigate our proposed solution, we first conducted a simple experiment. Specifically, we compare the number of UAVs needed for an initial network with 5 nodes to the same network after adding 5 more nodes to have a total of 10 nodes. We assume the same positions for the source and the destination nodes. The number of UAVs added for the first case (Fig. 4a) is 3 while it is 2 for the second case (in Fig. 4b), depending on the need of the network. Fig. 5 further investigates the UAV transmission range on the number of UAV needed in both 5 and 10 nodes network. As shown in the figure, the number of UAVs required decreases with the UAV range extension; and it settles to only 1 UAV when the range is almost covering the whole area.

Next, the achieved enhancement in the network algebraic connectivity is assessed before and after using the UAVs with the network growth. As seen in Fig. 6, the algebraic connectivity after adding the UAVs with optimal positioning is higher than that of the original network without the UAVs. The connectivity for our approach is enhanced by almost 200% at $N = 10$ and 66% at $N = 30$ compared to the original network.

Furthermore, the results depicted in Fig. 7 shows that the average number of UAVs needed tends to decrease with the increased number of nodes. That is due to increasing the number of nodes in the same area, and as a result, more links are created between original nodes and decreases the need for UAVs to support the network connectivity.

6.3.2. Routing performance

Next, we investigate the E2E delay and throughput performance for the proposed routing algorithm compared to the original network.

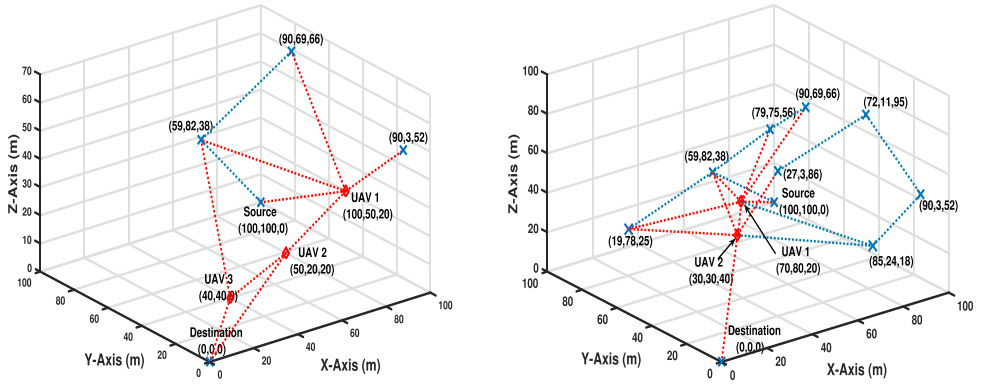

(a) $N = 5$ (b) $N = 10$

Fig. 4. UAV positioning for different number of nodes. The cross and diamond markers represent nodes and UAVs, respectively.

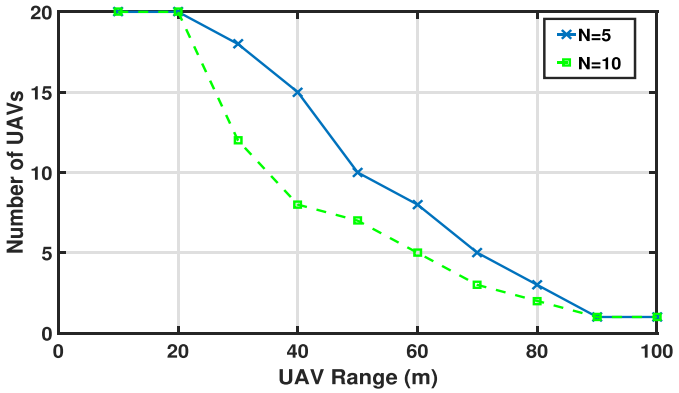

Fig. 5. The number of UAVs required for different UAV transmission range.

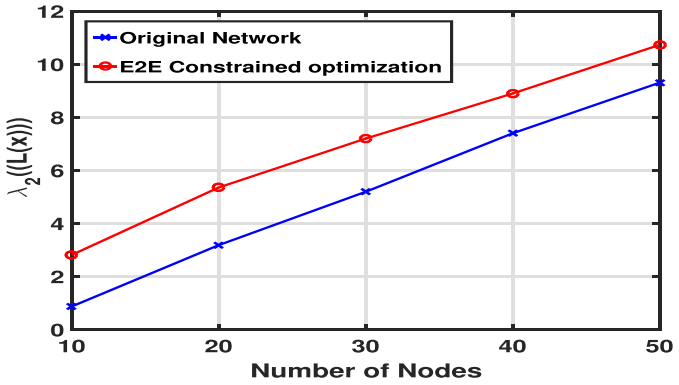

Fig. 6. The network connectivity enhancement through UAVs.

First, we study the performance of using a single path with the deployment of UAVs while parallel multi-paths are available. To this end, we fixed N to 50 and determined three node-disjoint paths (i.e., Path 1, Path 2, and Path 3) with the lowest E2E delay (from MATLAB results) from the same source and destination in the original network topology. We report the NS-3 results of the throughput (TP) and E2E delay per frame transmission for these paths when UDP is used as the transport layer protocol in Table 4.

The results show a significant improvement in both TP and E2E for the network after adding the UAVs. In some cases, the TP triples on average, and the E2E delay reduces to less than half. Because the UAVs are placed in locations that will reduce the E2E delay based on the proposed solution/ optimization. The decrease in E2E delay also enables increased TP. In addition,

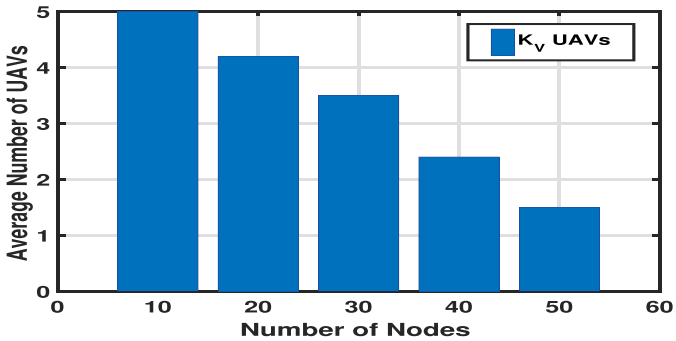

Fig. 7. Average number of UAVs needed for different N.

Table 4
Path performance comparison.

	Path 1	Path 2	Path 3
Original Network (No UAVs)			
TP (MB/s)	0.31	0.23	0.17
E2E (ms)	0.4664	0.63	0.83
Network with UAVs			
TP (MB/s)	0.73	0.58	0.8
E2E (ms)	0.20	0.25	0.18

Table 5
Original network packet delivery ratio.

MCS Index	Transmitted frames	Received frames	PDR (%)
Original network (No UAVs)			
10	2106	151	7
11	2106	679	32
12	2106	1697	81
18	2106	2106	100
Network with UAVs			
10–18	2106	2106	100

Table 6
UDP vs. TCP performance comparison.

	E2E (ms)	
Min. delay paths	UDP	TCP NewReno
Path 1	0.018	0.034
Path 2	0.015	0.025
Path 3	0.038	0.072

we speculate that the paths for the original network might have fewer hops and thus the longer distance between nodes, which impacts the packet delivery ratio (PDR) in mmWave links. That is not the case in our approach since the number of hops is increased while the distance between nodes decreased, which enables better PDR. Hence, we investigated the effect of the Modulation and Coding Scheme (MCS) index on the PDR for the baseline, original network, and our approach for $N = 10$ in Table 5. The results show that the original network has a high packet loss for the MCS index under 18, while the proposed optimal UAVs positioning optimization has no packet loss even with a low-quality MCS index. The reason behind high packet loss in the original network is that the nodes are long distanced, and the mmWave channel is lossy.

On the other hand, using TCP transmission may add extra overhead to the E2E delay due to the TCP handshake process for the network with UAVs. To investigate this point with transmitting of 10,000 packets with a packet rate of 4 MB/s and a packet interval of 16 μsec/packet for both UDP and TCP NewReno for $N = 50$. The results in Table 6 shows a lower E2E delay for the UDP connection due to the TCP setup process.

In the next experiment, we investigated the achieved enhancement in the E2E delay and TP between the source and destination nodes

As can be seen in Fig. 8(a), the multi-path approach uses parallel communication over both the hybrid path and the UAV-only path. Then, the E2E delay achieved will be equal to the minimum E2E delay of both paths. In other words, the receiver would pick the frame which arrives first. So in all cases, our proposed approach achieved the least E2E delay. The

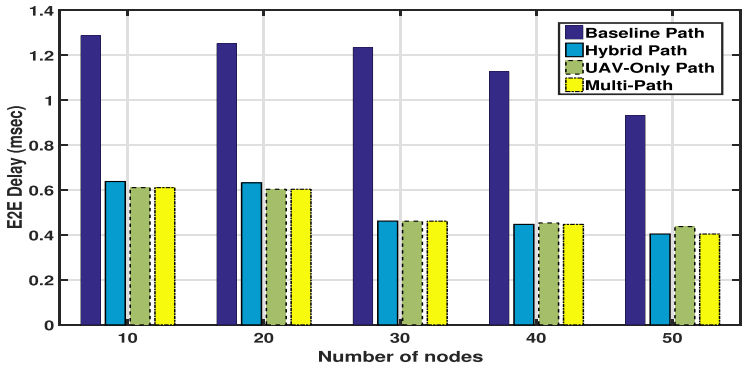

(a) The E2E delay.

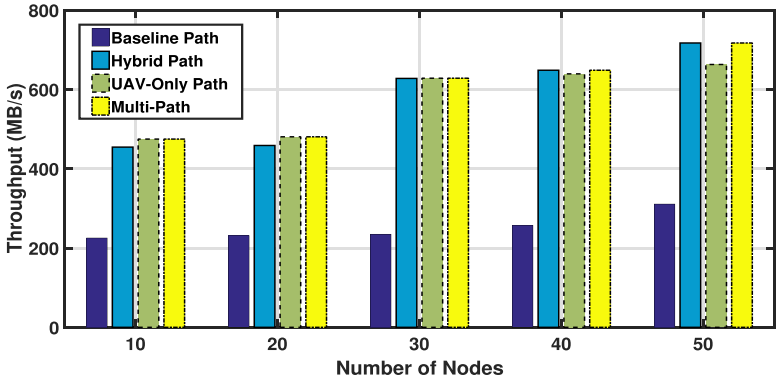

(b) The throughput.

Fig. 8. The E2E delay and throughput for different N.

improvement concerning no UAV-case (baseline) is particularly significant when the network size is smaller (i.e., above 50%) as there are no alternative path options for such smaller sizes. Comparing the Hybrid Path and UAV-only path, we see that the results are close to each other. But Hybrid Path performs better as the number of nodes increases, giving more path options to be used.

Looking at the TP in Fig. 8(b), we observe that it increases for the Hybrid Path approach as better paths are becoming available with the increased number of nodes. In such cases, our multi-path approach benefits from such an increase in terms of TP as it utilizes that path instead of the UAV-only one. The UAV-only path does not benefit from the growth of the network as it solely relies on UAVs. These results are consistent with the E2E delay results. As a result, we can conclude that the parallel multi-path approach performs the best in terms of E2E delay and TP in all cases, which indicates its effectiveness. These results further emphasize our model appropriateness for emergency management and first responder applications with high bandwidth streaming requirements.

On the other hand, multi-path parallel transmission adds an extra overhead by introducing redundant transmissions. However, these parallel transmissions are needed to guarantee the delivery and increase the overall throughput, as shown in the experiments aforementioned (Fig. 8). Hence, to justify our multi-path parallel transmission overhead, we conducted some experiments to include results on how TCP performance improves by reporting the number of re-transmissions compared to actual transmissions. For this set of experiments, we used the following TCP settings: TCP NewReno with a total of 10,000 transmitting packets with a packet rate of 4 MB/sec and a packet interval of 16 μsec/packet. As shown in Fig. 9, the baseline TCP re-transmissions are much higher than our proposed scheme even for the multi-path transmission. For example, at $N = 30$ nodes, the TCP re-transmissions are around 350 packets; but with our proposed scheme, it's around $50 - 60$ packets on the Uav-Only and the Hybrid paths. Moreover, even with the two parallel paths, the total TCP re-transmissions are just a little above 100 packets, which is almost 75% fewer re-transmissions.

6.3.3. Comparison of optimization and NS-3 results

An important factor in the evaluation is the accuracy of optimization results concerning a real-life situation. Thus, we compared the NS-3 results with other optimization results from MATLAB on the same topologies. Fig. 10 shows the E2E delay from the MATLAB optimization compared to the NS-3 simulator. As can be seen, the optimization results show slightly lower

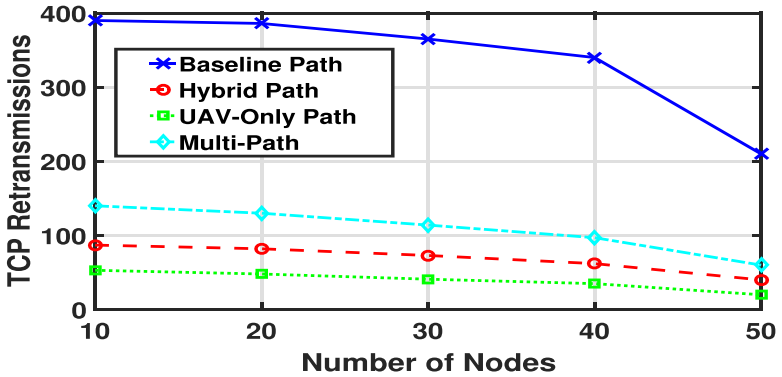

Fig. 9. TCP re-transmissions overhead for different *N*.

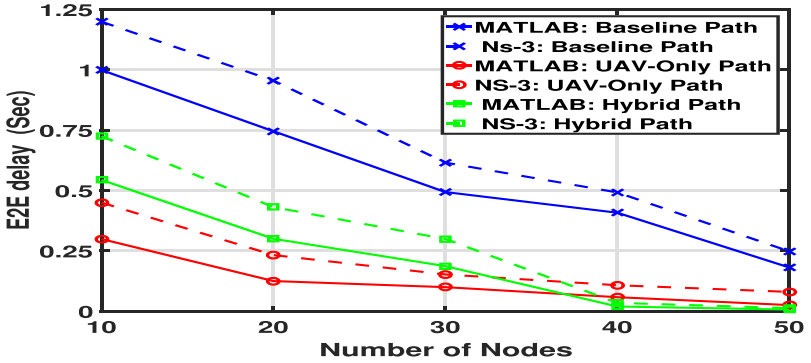

Fig. 10. Optimization vs NS-3 E2E delay for different *N*.

E2E delays since the deployment in a realistic environment faces uncertainties and complexities that could not be captured within analytical models. However, the trends match perfectly and indicate the validity of the optimization results. The slight difference can be attributed to various overheads in actual transmissions: For instance, the delay may be due to half-duplex operations in NS-3 and the processing delay at the receiver side when dealing with multiple redundant transmissions. In addition, the processing of packet headers at the receiver side adds to the total delay.

7. Conclusion

In this paper, we tackle the reliability problem of mmWave communications by deploying additional UAVs and exploiting parallel multi-path transmissions through the help of these UAVs. Specifically, we maximized the initial network connectivity under an E2E delay constraint and a maximum transmission power for the UAVs assuming IEEE 802.11ad-based connections. We then utilized a node-disjoint routing protocol that utilizes the mmWave PHY layer information and supports parallel multi-path transmissions for improved E2E delay and throughput performance.

The proposed multi-path routing protocol is implemented and tested on NS-3 by relying on the output from the optimization done in MATLAB. The results demonstrated the feasibility and effectiveness of multi-path routing in terms of achieving better throughput while minimizing the E2E delay. Moreover, the results show that the network connectivity enhanced by 66% after adding the UAVs, also the E2E delay is reduced by 50% to 66% depending on the number of nodes. Furthermore, the results show the dependency on the node numbers for both connectivity enhancement and E2E latency.

Declaration of Competing Interest

None.

Appendix A. Appendix I

Here, we investigate the delay performance for the packet transmit over each path of the multi-path communication with a total queue delay is,

$$D_q = \min_M \left(\sum_{n=1}^{N'} W_N + W_s \right) \tag{A.1}$$

where D_q is the total queuing delay at any node i and W_s is the total queuing delay at the source node. Furthermore, calculating the total queuing delay for each path requires the queuing delay for each node in that path, hence, the need for queuing analysis at each node.

A0.4. Source node with M/G/1 queue

We begin the queuing analysis with the queuing model at the source node with the $M/G/1$ model shown in Fig. 3. The $M/G/1$ waiting delay at the source node is as follows [53],

$$W_{q,s} = \frac{\lambda_i(\sigma_{s,i}^2 + \mathbf{E}\{Z\}^2)}{2(1-\rho)}, \tag{A.2}$$

where λ_i, $\mathbf{E}\{Z\}$ and $\sigma_{s,i}^2$ are the arriving rate to the queue, the service process expectation and the service process variance at node i which is the source node in this case, respectively. Moreover, $\rho = \lambda_i/\mu_i$ is the service utilization, where μ_i is the service rate of the queue and $0 \leq \rho < 1$. Then, the total queue delay at node s is,

$$W_s = W_{q,s} + \frac{1}{\mu_i}. \tag{A.3}$$

Furthermore, the service process in this model is depending on the mmWave channel statistics and the probability distribution density function (PDF) of proper transmission. In this work, we utilize the 10° transmit antenna. The relative strength of both the direct and the scattered components of the received signal is expressed by the K-factor with a Rician distribution [54,55]. The K-factor provides an indication of link quality and the received power in a reach scattering environment. Hence, the K-factor is fitted to a Gaussian distribution with mean of $\mathbf{E}\{X\}$ and variance of σ_X where $X = P_{Rx}$ of $\mathcal{P}rob\{X \leq P_{th}\}$ where P_{th} is the threshold received power for a proper communication.

A0.5. Nodes with G/G/1 queue

Now, we investigate the queuing analysis with the queuing model at all other nodes with the $G/G/1$ model shown in Fig. 3. The $G/G/1$ waiting delay is following Kingman's formula [56], which is an approximation formula for the mean waiting time in a $G/G/1$ queue and is known to be generally very accurate. Then, the queue waiting time at any node i is as follows

$$W_{q,i} = \frac{\rho_i}{1-\rho_i} \cdot \frac{C_a^2 + C_s^2}{2} \cdot \frac{1}{\mu_i}, \tag{A.4}$$

where $\rho_i = \lambda_i/\mu_i$ is the service utilization and C_a and C_s are the coefficient of variation for the arrival and service processes, respectively. The coefficient of variation is a standardized measure of the dispersion of random variable g a probability distribution function and equal to the standard deviation of the distribution divided by its mean, $C = \sigma_g/\mathbf{E}\{g\}$.

Then the queue waiting time can be approximated as follows

$$W_{q,i} = \sigma_Y^2 \left(\frac{d_{r,i}}{d_{s,i}|d_{s,i} - d_{r,i}|} \right)^n. \tag{A.5}$$

is a linear function of the distances. Then, the total delay at any node N (except the source node s) is,

$$W_i = \sigma_Y^2 \left(\frac{d_{r,i}}{d_{s,i}|d_{s,i} - d_{r,i}|} \right)^n + \mathbf{E}\{Y\} d_{s,i}^{-n}. \tag{A.6}$$

Appendix B. Appendix II

In order to establish convexity of the constraints of the proposed optimization problem, the following constraints are linear so no need for further convex investigation,

$$\begin{aligned} &\mathbf{x}^T \mathbf{d}_{i,j} \leq R, \\ &\textstyle\sum_{q=1}^{Q_V} P_q \leq P_V, \\ &\mathbf{1}^T \mathbf{x} <= K_V, \ \ \mathbf{x} \in [0,1]. \end{aligned} \tag{B.1}$$

Hence, we only need to establish the convexity of the E2E delay constraint with respect to the optimization variables, $\mathbf{x}$, $\log(P_q)$, and K_V. Moreover, as aforementioned in Section 5.1 the problem is solved for one UAV at a time, then the optimization variables that affect the optimization are only $\mathbf{x}$ and $\log(P_q)$.

From Eq. (4), the E2E delay, D_{E2E}, is given by:

$$D_{E2E} = D_t + D_p + D_q, \tag{B.2}$$

where,

$$D_t = N' \frac{m}{\min_{\{i,j\} \in \mathbf{s}} R_{i,j}}, \tag{B.3}$$

$$D_p = \frac{\sum_{\{i,j\}\in \mathbf{S}}^{N'} \|\mathbf{u}_i - \mathbf{u}_j\|_2}{c}, \tag{B.4}$$

$$D_q = \sum_{i=1}^{N'} W_i + W_s. \tag{B.5}$$

Furthermore, the E2E delay has three terms, it suffices to prove that each term is convex in $\mathbf{x}$ and $\log(P_q)$; this follows from the fact that the sum of convex functions is also convex [57]. We can validate the convexity of D_{E2E} by examining the Hessian of each term. The hessian matrix for two optimization variables is as follows

$$\mathbf{H}_n(\mathbf{x}, \log(P_q)) = \begin{bmatrix} \frac{\delta^2 F(\mathbf{x},\log(P_q))}{\delta \mathbf{x}^2} & \frac{\delta^2 F(\mathbf{x},\log(P_q))}{\delta \mathbf{x} \delta \log(P_q)} \\ \frac{\delta^2 F(\mathbf{x},\log(P_q))}{\delta \log(P_q) \delta \mathbf{x}} & \frac{\delta^2 F(\mathbf{x},\log(P_q))}{\delta \log(P_q)^2} \end{bmatrix}, \tag{B.6}$$

if the hessian matrix of a function is positive semi-definite in the optimization variables, $\mathbf{H}_n(\mathbf{x}, \log(P_q)) \succeq 0$, that means it is a convex function. Also, if the hessian matrix of a function is negative definite in the optimization variables, $\mathbf{H}_n(\mathbf{x}, \log(P_q)) \preceq 0$, that means it is a concave function.

First for D_t in Eq. (B.3), from the convex set properties the function $1/f(x)$ is convex if and only if the function $f(x)$ is a function convexity preserving and its interior is also convex.

The min function is a convexity preserving function [57], i.e., we only need to prove that the interior function, $R_{i,j}$, is convex. The $R_{i,j}$ can be written as

$$\begin{aligned} R_{uav,j} \leq W \Big[& \log_2(P_q) + 2\log_2(|h_{i,r}|) - n\log(d_{uav,j}) \\ & - \log_2\left(\textstyle\sum_{j=1, j\neq i}^{N} \exp^{P_q |h_{i,r}|^2 d_{j,r}^{-n}}\right) - \log(\sigma_0^2), \Big] \end{aligned} \tag{B.7}$$

Whereas, the only rate, $R_{i,j}$, that depend on the UAV location and power are the links that connects the nodes through the UAV Then, applying the hessian matrix on Eq. (B.7)$\mathbf{H}_n(D_{Tx}(\mathbf{x}, \log(P_q)))$, then the function is convex as it can be shown as a zero matrix, Which indicate that it is a linear function, hence, $R_{i,j}$ is convex. Second, we inspect D_P which can be written as follows

$$D_p = \frac{\sum_{\{i,j\}\in \mathbf{S}}^{N'} \mathbf{x}^T \mathbf{D}_{i,j}}{c} \tag{B.8}$$

where, $\mathbf{D}_{i,j} \in \mathbf{R}^{\beta \times N}$ is the quantized distances between any 2 nodes i and j. Moreover, this term is linear $\mathbf{x}$, hence, it is convex. The convex investigation for the queue delay model is a quadratic function of the distances. Furthermore, the convexity investigation for D_p fit for the second and third constraints in Eq. (19), is a linear constraint as it sums over $\log(P_q)$. Moreover, D_q is a positive quadratic function in $\mathbf{x}$ and $\log(P_q)$.

References

[1] C.X. Wang, A. Ghazal, B. Ai, Y. Liu, P. Fan, Channel measurements and models for high-speed train communication systems: a survey, IEEE Commun. Surveys Tutorials 18 (2) (2016) 974–987.
[2] K. Werbach, A. Mehta, The spectrum opportunity: sharing as the solution to the wireless crunch, Int. J. Commun. 8 (2014) 22.
[3] R.A. DiFazio, P.J. Pietraski, The bandwidth crunch: can wireless technology meet the skyrocketing demand for mobile data? in: Proceedings of the IEEE Long Island Systems, Applications and Technology Conference, 2011, pp. 1–6.
[4] L. Wei, R.Q. Hu, Y. Qian, G. Wu, Key elements to enable millimeter wave communications for 5G wireless systems, IEEE Wirel. Commun. 21 (6) (2014) 136–143.
[5] S. Geng, J. Kivinen, X. Zhao, P. Vainikainen, Millimeter-wave propagation channel characterization for short-range wireless communications, IEEE Trans. Vehic. Technol. (TVT) 58 (1) (2009) 3–13.
[6] E. Ben-Dor, T.S. Rappaport, Y. Qiao, S.J. Lauffenburger, Millimeter-wave 60 GHz outdoor and vehicle AOA propagation measurements using a broadband channel sounder, in: Proceedings of the IEEE Global Telecommunications Conference (GLOBECOM), 2011, pp. 1–6.
[7] T.S. Rappaport, S. Sun, R. Mayzus, H. Zhao, Y. Azar, K. Wang, G.N. Wong, J.K. Schulz, M. Samimi, F. Gutierrez, Millimeter wave mobile communications for 5G cellular: it will work!, IEEE Access 1 (2013) 335–349.
[8] X. Wu, C.X. Wang, J. Sun, J. Huang, R. Feng, Y. Yang, X. Ge, 60-GHz millimeter-wave channel measurements and modeling for indoor office environments, IEEE Trans. Antennas Propag. 65 (4) (2017) 1912–1924.
[9] W. Roh, J.Y. Seol, J. Park, B. Lee, J. Lee, Y. Kim, J. Cho, K. Cheun, F. Aryanfar, Millimeter-wave beamforming as an enabling technology for 5G cellular communications: theoretical feasibility and prototype results, IEEE Commun. Mag. 52 (2) (2014) 106–113.
[10] A. Thornburg, R.W. Heath, Capacity and coverage in clustered LoS mmwave ad hoc networks, in: Proceedings of the IEEE Global Communications Conference (GLOBECOM), 2016, pp. 1–6.
[11] R. Bishop, A survey of intelligent vehicle applications worldwide, in: Proceedings of the IEEE Intelligent Vehicles Symposium (Cat. No.00TH8511), 2000, pp. 25–30.
[12] B. Braunstein, T. Trimble, R. Mishra, B. Manoj, L. Lenert, R. Rao, Challenges in using distributed wireless mesh networks in emergency response, in: Proceedings of the Third International ISCRAM Conference, 2006, pp. 30–38.
[13] H. Assasa, J. Widmer, Implementation and evaluation of a WLAN IEEE 802.11 ad model in ns-3, in: Proceedings of the ACM Proceedings of the Workshop on ns-3, 2016, pp. 57–64.
[14] N. Rupasinghe, A.S. Ibrahim, I. Guvenc, Optimum hovering locations with angular domain user separation for cooperative UAV networks, in: Proceedings of the IEEE Global Communications Conference (GLOBECOM), 2016, pp. 1–6.
[15] M.M. Azari, F. Rosas, K.C. Chen, S. Pollin, Optimal UAV positioning for terrestrial-aerial communication in presence of fading, in: Proceedings of the IEEE Global Communications Conference (GLOBECOM), 2016, pp. 1–7.

[16] S. Mignardi, R. Verdone, On the performance improvement of a cellular network supported by an unmanned aerial base station, in: Proceedings of the International Teletraffic Congress (ITC), 2, 2017, pp. 7–12.
[17] G.J. Lim, S. Kim, J. Cho, Y. Gong, A. Khodaei, Multi-UAV pre-positioning and routing for power network damage assessment, IEEE Trans. Smart Grid PP (99) (2016) 1-1.
[18] Z. Dejin, N. Yang, W. Liaoni, Z. Shenglu, A kind of moving net recovery technology for unmanned aerial vehicle, in: Proceedings of the International Conference on Information and Communications Technologies (ICT), 2015, pp. 1–5.
[19] S.Y. Park, D. Jeong, C.S. Shin, H. Lee, DroneNet+: adaptive route recovery using path stitching of UAVs in Ad-Hoc networks, in: Proceedings of the IEEE Global Communications Conference (GLOBECOM), 2017, pp. 1–7.
[20] S. Rohde, C. Wietfeld, Interference aware positioning of aerial relays for cell overload and outage compensation, in: Proceedings of the IEEE Vehicular Technology Conference (VTC), 2012, pp. 1–5.
[21] M. Mozaffari, W. Saad, M. Bennis, M. Debbah, Unmanned aerial vehicle with underlaid device-to-device communications: performance and tradeoffs, IEEE Trans. Wireless Commun. 15 (6) (2016) 3949–3963.
[22] M. Mozaffari, W. Saad, M. Bennis, M. Debbah, Drone small cells in the clouds: design, deployment and performance analysis, in: Proceedings of the IEEE Global Communications Conference (GLOBECOM), 2015, pp. 1–6.
[23] E. Kalantari, M.Z. Shakir, H. Yanikomeroglu, A. Yongacoglu, Backhaul-aware robust 3D drone placement in 5G+ wireless networks, in: Proceedings of the IEEE International Conference on Communications Workshops (ICC Workshops), 2017, pp. 109–114.
[24] L. Kong, L. Ye, F. Wu, M. Tao, G. Chen, A.V. Vasilakos, Autonomous relay for millimeter-wave wireless communications, IEEE J. Sel. Areas Commun. 35 (9) (2017) 2127–2136.
[25] W. Khawaja, O. Ozdemir, I. Guvenc, UAV air-to-ground channel characterization for mmWave systems, in: Proceedings of the 2017 IEEE 86th Vehicular Technology Conference (VTC-Fall), 2017, pp. 1–5.
[26] Z. Xiao, P. Xia, X. Xia, Enabling UAV cellular with millimeter-wave communication: potentials and approaches, IEEE Commun. Mag. 54 (5) (2016) 66–73.
[27] M.A. Abdel-Malek, A.S. Ibrahim, M. Mokhtar, Optimum UAV positioning for better coverage-connectivity tradeoff, in: Proceedings of the IEEE International Symposium on Personal, Indoor, and Mobile Radio Communications (PIMRC), 2017, pp. 1–5.
[28] M.A. Abdel-Malek, A.S. Ibrahim, M. Mokhtar, K. Akkaya, UAV positioning for out-of-band integrated access and backhaul millimeter wave network, Physical Communication 35 (2019) 100721.
[29] J. He, J. Rexford, Toward internet-wide multipath routing, IEEE Netw. 22 (2) (2008) 16–21.
[30] and, and, Multipath source routing in wireless ad hoc networks, in: Proceedings of the 2000 Canadian Conference on Electrical and Computer Engineering. Conference Proceedings. Navigating to a New Era (Cat. No.00TH8492), 1, 2000, pp. 479–483.
[31] J. Chen, P. Druschel, D. Subramanian, An efficient multipath forwarding method, in: Proceedings of IEEE INFOCOM'98, the Conference on Computer Communications. Seventeenth Annual Joint Conference of the IEEE Computer and Communications Societies. Gateway to the 21st Century, 3, 1998, pp. 1418–1425.
[32] I. Cidon, R. Rom, Y. Shavitt, Analysis of multi-path routing, IEEE/ACM Trans. Netw. 7 (6) (1999) 885–896.
[33] A. Nasipuri, S.R. Das, On-demand multipath routing for mobile ad hoc networks, in: Proceedings of the Eight International Conference on Computer Communications and Networks (Cat. No.99EX370), 1999, pp. 64–70.
[34] M.K. Marina, S.R. Das, On-demand multipath distance vector routing in ad hoc networks, in: Proceedings of the Ninth International Conference on Network Protocols (ICNP), 2001, pp. 14–23.
[35] M.K. Marina, S.R. Das, Ad hoc on-demand multipath distance vector routing, Wireless communications and mobile computing 6 (7) (2006) 969–988.
[36] X. Huang, Y. Fang, Performance study of node-disjoint multipath routing in vehicular ad hoc networks, IEEE Trans. Veh. Technol. 58 (4) (2009) 1942–1950.
[37] S.-J. Lee, M. Gerla, Split multipath routing with maximally disjoint paths in ad hoc networks, in: Proceedings of the IEEE International Conference on Communications (ICC), 10, 2001, pp. 3201–3205 vol.10.
[38] X. Li, L. Cuthbert, On-demand node-disjoint multipath routing in wireless ad hoc networks, in: Proceedings of the 29th Annual IEEE International Conference on Local Computer Networks, 2004, pp. 419–420.
[39] X. Li, L. Cuthbert, Stable node-disjoint multipath routing with low overhead in mobile ad hoc networks, in: Proceedings of the IEEE Computer Society's 12th Annual International Symposium on Modeling, Analysis, and Simulation of Computer and Telecommunications Systems (MASCOTS). Proceedings., 2004, pp. 184–191.
[40] X. Huang, Y. Fang, Performance study of node-disjoint multipath routing in vehicular ad hoc networks, IEEE Trans. Veh. Technol. 58 (4) (2009) 1942–1950.
[41] M. Radi, B. Dezfouli, K.A. Bakar, M. Lee, Multipath routing in wireless sensor networks: survey and research challenges, Sensors 12 (1) (2012) 650–685.
[42] S. Sun, G.R. MacCartney, T.S. Rappaport, A novel millimeter-wave channel simulator and applications for 5G wireless communications, in: Proceedings of the IEEE International Conference on Communications (ICC), 2017, pp. 1–7.
[43] J.F. Kurose, K.W. Ross, Computer Networking: a Top-Down Approach, Addison-Wesley Reading, 2010.
[44] D.P. Bertsekas, R.G. Gallager, Data Networks, Prentice Hall, pp. 187–188.
[45] M. Fiedler, Algebraic connectivity of graphs, Czechoslov. Math. J. 23 (2) (1973) 298–305.
[46] M. Grant, S. Boyd, Y. Ye. (2008). CVX: Matlab software for disciplined convex programming.
[47] M. Polese, R. Jana, M. Zorzi, TCP and MP-TCP in 5G mmWave networks, IEEE Internet Comput. 21 (5) (2017) 12–19.
[48] D.B. Johnson, D.A. Maltz, Dynamic source routing in ad hoc wireless networks, in: Mobile Computing, Springer, 1996, pp. 153–181.
[49] D.B. Johnson, D.A. Maltz, J. Broch, et al., DSR: the dynamic source routing protocol for multi-hop wireless ad hoc networks, Ad hoc Netw. 5 (2001) 139–172.
[50] B.S. Davie, Y. Rekhter, MPLS: Technology and Applications, Morgan Kaufmann Publishers Inc., 2000.
[51] Xipeng Xiao, A. Hannan, B. Bailey, L.M. Ni, Traffic engineering with MPLS in the internet, IEEE Netw. 14 (2) (2000) 28–33.
[52] J. Klaue, B. Rathke, A. Wolisz, valVid – a framework for video transmission and quality evaluation, in: Computer Performance Evaluation. Modelling Techniques and Tools, Springer Berlin Heidelberg, 2003, pp. 255–272.
[53] G. Jain, K. Sigman, A Pollaczek–Khintchine formula for M/G/1 queues with disasters, J. Appl. Probab. 33 (4) (1996) 1191–1200.
[54] C. Tepedelenlioglu, A. Abdi, G.B. Giannakis, The Ricean K factor: estimation and performance analysis, IEEE Trans. Wireless Commun. 2 (4) (2003) 799–810.
[55] N.F. Abdullah, D. Berraki, A. Ameen, S. Armour, A. Doufexi, A. Nix, M. Beach, Channel parameters and throughput predictions for mmWave and LTE-A networks in urban environments, in: Proceedings of the IEEE Vehicular Technology Conference (VTC Spring), 2015, pp. 1–5.
[56] J. Kingman, The single server queue in heavy traffic, in: Mathematical Proceedings of the Cambridge Philosophical Society, Cambridge University Press, 1961, pp. 902–904.
[57] S. Boyd, L. Vandenberghe, Convex Optimization, Cambridge University Press, 2004.